2018

Fe-Si networks and charge/discharge-induced phase transitions in Li2FeSiO4 cathode materials

Xiaobao Lv
Ames Laboratory

Xin Zhao
Ames Laboratory, xzhao@iastate.edu

Shunqing Wu
Xiamen University

Manh Cuong Nguyen
Ames Laboratory, mcnguyen@ameslab.gov

Zizhong Zhu
Xiamen University

See next page for additional authors

Fe-Si networks and charge/discharge-induced phase transitions in Li2FeSiO4 cathode materials

Abstract
Structural phase transitions of electrode materials are responsible for poor reversibility during charge/discharge cycling in Li-ion batteries. Using previously developed structural databases, we investigate a structural landscape for LixFeSiO4systems at x = 1. Starting with low-energy Li2FeSiO4 crystal structures, we explore the crystal structures of the material in different states of charge. The as-prepared Li2FeSiO4 materials adopt low energy structures characterized by two-dimensional (2D) Fe–Si networks. After the removal of one Li per formula unit to form LiFeSiO4, the structures with three-dimensional (3D) diamond-like Fe–Si networks become more energetically favorable without a significant impact on the charge capacity, which agrees with previous experimental and theoretical work. However, we reveal that the structure with a 3D diamond-like Fe–Si network can further transform into a new structure at x = 1. And the Li atom is hard to reinsert into these new structures. Consequently the system is prevented from returning to the Li2FeSiO4 state. We believe that the formation of this new structure plays an important role in the loss of reversible capacity of Li2FeSiO4 electrode materials.

Disciplines
Inorganic Chemistry | Materials Chemistry

Authors
Xiaobao Lv, Xin Zhao, Shunqing Wu, Manh Cuong Nguyen, Zizhong Zhu, Zijing Lin, Cai-Zhuang Wang, and Kai-Ming Ho

PCCP

PAPER

Fe-Si networks and charge/discharge-induced phase transitions in Li_2FeSiO_4 cathode materials

Received 00th January 20xx,
Accepted 00th January 20xx

DOI: 10.1039/x0xx00000x

www.rsc.org/

Xiaobao Lv[ab], Xin Zhao[b], Shunqing Wu[c], Manh Cuong Nguyen[b], Zizhong Zhu[c], Zijing Lin*[a], Cai-Zhuang Wang[b], and Kai-Ming Ho*[de]

Structural phase transitions of electrode materials are responsible for poor reversibility during charge/discharge cycling in Li-ion batteryies. Using previously-developed structural databases, we investigate the structural landscape for Li_xFeSiO_4 systems at x=1. Starting with the low-energy Li_2FeSiO_4 crystal structures, we explore the crystal structures of the material at different state of charge. As-prepared Li_2FeSiO_4 materials adopt low energy structures characterized by two-dimensional (2D) Fe-Si networks. After removal of one Li per formula unit to form $LiFeSiO_4$, the structures with three-dimensional (3D) diamond-like Fe-Si networks become more energetically favorable without significant impact on the charge capacity, which agrees with previous experimental and theoretical work. However, we reveal that the structure with 3D diamond-like Fe-Si network can further transform to a new structure at *x*=1. And Li atom is hard to reinsert into these new structures. Consequently the system is prevented from returning to the Li_2FeSiO_4 state. We believe formation of this new structure plays an important role in the loss of reversible capacity of Li_2FeSiO_4 electrode material.

1. Introduction

Lithium iron silicate, *i.e.* Li_2FeSiO_4, is a promising cathode material for advanced Li-ion batteries due to its high theoretical capacity, low cost and environmental friendliness [1,2]. Despite its theoretical capacity (~331 mAh/g) for extracting 2 Li atoms per formula unit (f.u.), early experimental reversible capacity only reaches half of the theoretical value (130 ~ 165 mAh/g, corresponding to Li_xFeSiO_4, x=1~1.2)[1,3,4]. In subsequent work, reversible capacity over 200 mAh/g has been reported, extending the delithiated composition to x<0.8 [5–7]. Recently, Ti doped Li_2FeSiO_4/C was reported with a capacity over 300 mAh/g which almost reached the theoretical capacity[8]. Extending the range and stability of the material under repeated cycling is still a key issue. Hence, studying the structural transition mechanisms that may potentially damage the capacity and limit the reversible x range in Li_xFeSiO_4 during cycling becomes very important.

Currently, the Li-Fe site exchange process is the most well-known mechanism that causes phase transitions in this material. This mechanism changes the local environment of FeO_4 tetrahedron and Li diffusion path, resulting in a change in voltage [9–12]. Experimental results of the Li_2FeSiO_4/$LiFeSiO_4$ cycling show irreversible voltage plateau change from ~3.1V (first cycle) to ~2.8V (subsequent cycles) due to structural transitions at the end of the first cycle. This lowering of the potential plateau has been ascribed to the Li-Fe site-exchange mechanism which happens at 4b Li sites and 2a Fe sites in the $Pmn2_1$ experimental phase by Nytén et al [9]. Later, Armstrong *et al.* [3] and Kojima *et al.* [13] reported two cycled phases for the experimental phases of $Pmn2_1$ and $P2_1/n$, respectively. Li *et al.* [10] investigated the 3D site-exchanged Pmn21-cycled phase and found the fully delithiated $FeSiO_4$ composition is rather brittle as the cell expanded significantly comparing the 2D phase. Several theoretical studies confirmed the voltage shift between the as-prepared phases and the cycled phases [11, 14–16]. Saracibar *et al.*'s first principles study of the half delithiated $LiFeSiO_4$ composition shows that the 3D Fe-O-Si frameworks are more energetically favourable than the 2D Fe-O-Si frameworks, which results in a thermodynamic driving force for the structural transition from 2D to 3D upon delithiation [15].

Previous experimental or theoretical studies focusing on Li_2FeSiO_4/$LiFeSiO_4$ cycling show no significant capacity loss when Li-Fe site-exchanges occur except for a voltage change when the 3D type Li_2FeSiO_4 forms [9,17]. The experimentally observed reversible capacity over 200 mAh/g [5–7] indicates more than one lithium per f.u. of Li_2FeSiO_4 can be reversibly extracted/inserted. Investigating Li removal beyond x=1, Zhang *et al.*[11] found in first principles calculation an unexpected shift of the valence-change element from Fe to O when more than one Li ion is removed per f.u.. In this scenario, O^{2-} becoming O^- may lead to the possibility that O^- further transforms to O_2 gas and irreversibly transform Li_xFeSiO_4 into other phases and

[a] *CAS Key Laboratory of Strongly-Coupled Quantum Matter Physics, Department of Physics, University of Science and Technology of China, Hefei 230026, China. E-mail: zjlin@ustc.edu.cn*
[b] *Ames Laboratory, US DOE, Ames, Iowa 50011, USA.*
[c] *Collaborative Innovation Center for Optoelectronic Semiconductors and Efficient Devices, Department of Physics, Xiamen University, Xiamen 361005, China.*
[d] *International Center for Quantum Design of Functional Materials (ICQD), Hefei National Laboratory for Physical Sciences at the Microscale, University of Science and Technology of China, Hefei 230026, China.*
[e] *Department of Physics and Astronomy, Iowa State University, Ames, Iowa 50011, USA. E-mail: kmh@iastate.edu*

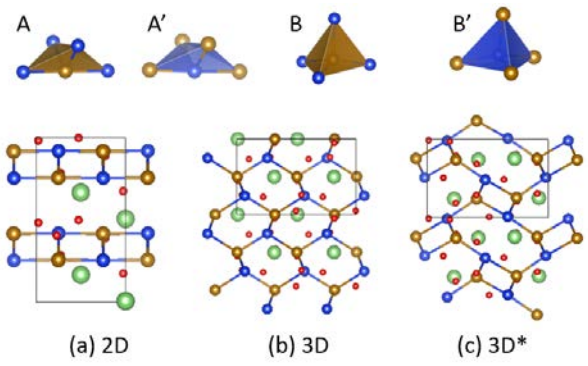

Fig. 1 Examples of 3 different Fe-Si networks and their building blocks in low-energy LiFeSiO4 structures (a) 2D Fe-Si network consists of building blocks A and A'. The Fe-Si network forms 2D stacking layers where Li atoms move between layers. (b) 3D Fe-Si network consists of building blocks B and B'. The Fe-Si atoms form a diamond-like 3D network where Li atoms can only move along 3D paths. (c) Another 3D Fe-Si network consists of building blocks B and A'. In all the structural figures in this paper, Li atoms are colored with light green, Fe atoms colored with brown, Si atoms are colored with blue, O atoms are colored with red.

damage the capacity. However, their calculations showed that $Li_{0.5}FeSiO_4$ is still stable and the release of O_2 is energetically unfavourable for removal of Li up to x=0.5. This provide support for reversible charging of Li_2FeSiO_4 up to a theoretical capacity of ~250 mAh/g in agreement with reports of cyclable performance reported in some Li_2FeSiO_4 batteries[17]. Furthermore, not all materials achieved this high-level performance and even the best materials suffer from a gradual capacity fade with repeated cycling. This suggests that there may be other mechanisms at work contributing to the performance degradation with cycling.

In this work, we propose a new capacity-damaging mechanism that exists in the middle of the charge/discharge cycle. We discover this mechanism through an extensive investigation of structural transitions that can occur in the Li_xFeSiO_4 system at x=1. To efficiently explore the low-energy structural landscape of $LiFeSiO_4$, we utilized structural databases we previously developed, including the one for Li_2FeSiO_4 using Motif-network scheme [18] and that for $LiFePO_4$ using Fe-P network-generation scheme [19]. We show that substitution of P atoms in low-energy $LiFePO_4$ structures with Si produce low-energy structural candidates for $LiFeSiO_4$. Energetic ordering between structures within FeO_4 and FeO_6 families are quite well preserved, indicating that the $LiFePO_4$ crystal structure database is a good guide to explore $LiFeSiO_4$ structures because both SiO_4 and PO_4 exhibit strong tetrahedral motifs. We found that some of the new low-energy substituted $LiFeSiO_4$ phases have no more "comfortable" room for extra Li atoms (extra Li atoms cannot form LiO_4 tetrahedron which is a common motif in low-energy Li_2FeSiO_4 structures). These new substituted $LiFeSiO_4$ phases can be more energetically favourable than delithiated structures from Li_2FeSiO_4. Phase transitions into these substituted $LiFeSiO_4$ structures can act as traps preventing the system from recovering to the initial Li_2FeSiO_4 condition, which cause a loss in reversible charging capacity in the cathode. First-principles studies are performed in this paper to support our hypothesis.

We use a new angle to study the Li_xFeSiO_4 system which focuses on the Fe-Si networks. The concept of Fe-Si network has been proposed by Ye et al. when studying the experimental X-ray diffraction data of Na_2FeSiO_4 battery materials during charge/discharge cycling [20]. A common diamond-like Fe-Si network was found for most of the low-energy structures of Na_2FeSiO_4. The electrochemical properties are also related to the type of Fe-Si networks: crystal structures with common Fe-Si networks have similar electrochemical behaviour from first principles calculations [21]. The concept has been generalized to $LiFePO_4$ systems by Lv *et al.* where Fe-P networks are used to predict new low-energy structures with remarkable success [19]. Following previous work[21], the Fe-Si networks in low-energy $LiFeSiO_4$ structures are classified into 2D-ladder-like, 3D-diamond-like and 3D*-4-8-membered-rings types (For simplicity, we use name "2D", "3D" and "3D*" in the following discussion) according to the $FeSi_4$ and $SiFe_4$ polyhedra which are considered as building blocks of the Fe-Si networks (fig.1).

2. Computational Methods

Density Functional Theory (DFT) calculations are performed using Vienna ab-initio simulation package (VASP) [22] with Perdew-Burke-Ernzerhof (PBE)[23] exchange-correlation functional. GGA+U method is used with an effective U_{eff}=U-J=4 eV for Fe atoms[24]. K-points resolution is $2\pi\times0.03$ Å^{-1} using Monkhorst-Pack scheme[25] and energy cut-off is 520 eV. Forces convergence criteria is set to 0.01 eV/Å in the structure relaxation and Nudged Elastic Band method[26] for phase transition barrier calculations. Crystal structure figures are plotted with VESTA[27].

3. Results and discussions

Our $LiFeSiO_4$ crystal structure data come from two sources. One is based on our previous Li_2FeSiO_4 structural database where motif-guided decoration of four-coordinated networks is used to generate many low-energy structures including all experimentally reported structures [18]. These Li_2FeSiO_4 structures are converted to $LiFeSiO_4$ structures by removal of one Li atom per f.u.. This pool represents structures which can return to the fully lithiated compound (x=2) by inserting back the Li atoms. The other source is based on the low-energy $LiFePO_4$ crystal structures generated using Fe-P networks[19]. Low-energy structures in the $LiFePO_4$ pool are substituted with Si on the P sites to get the $LiFeSiO_4$ structures, which may or may not be fully recovered to Li_2FeSiO_4. Both of the two sources of crystal database are valuable to our study as many new (hypothetical) structures have never been reported before.

3.1 Source I. Generation of the delithiated phases

Crystal structures of A_2MSiO_4 (A=Li, Na, M=Fe, Mn, Co) including Li_2FeSiO_4 have a common feature that each atom has 4 nearest neighbours and they form a 4-connected atom network in the cell space. Such 4-connected atom networks are commonly seen in zeolites, silicates and silicon. Based on such features, Zhao *et al.* generated a large amount of low-energy A_2MSiO_4 structures by assigning the A, M, Si and O atoms to the sites of 4-connected silicon networks. To obtain low-energy structures with reduced efforts, each O atom is forced to have 2 A, 1 M, 1 Si as nearest neighbours. More details can be found in the literature [18]. We select all low-energy Li_2FeSiO_4 structures in the energy range of 0~0.05 eV/f.u. above ground state as the starting population to perform the delithiation and the Li-Fe site exchange operations. Among them, five structures are experimental phases of Li_2FeSiO_4, the other five ones including the ground state are new structures.

To study the various possibilities of Li-Fe Site-Exchange situations, we treat all the Li and Fe atoms in a Li_2FeSiO_4 structure as equivalent sites, and re-assign them with equal amounts of vacancies, Li atoms and Fe atoms. For a 4 f.u. Li_2FeSiO_4 structure with 12 Li/Fe (8 Li + 4 Fe atoms) sites, there are theoretically $\boldsymbol{C_{12}^4 \times C_8^4 \times C_4^4 = 34650}$ possible arrangements for the 4 vacancies, 4 Li and 4 Fe atoms neglecting the symmetry of the structures. To reduce the large number of possibilities that need to be screened, we adopted a generalization of the empirical rule Zhao et al. discovered for low-energy Li_2FeSiO_4 structures. For Li_2FeSiO_4, the cations are uniformly distributed around oxygen atoms (i.e. each O atom is surrounded by 2 Li atoms, 1 Fe atom and 1 Si atom). Therefore, we assume that after delithiating half of the Li atoms, the cations should also be uniformly distributed (i.e. each O atom is surrounded by 1 Li atom, 1 Fe atom and 1 Si atom and 1 vacancy, see fig.2). We examined this rule on 20 Li_2FeSiO_4 structures with lowest-energy, their oxygen atoms are all surrounded with 4 atoms (2 Li + 1 Fe + 1 Si, see fig.2 left). After removing half Li atoms, each of the 20 structures produces 10~20 $LiFeSiO_4$ configurations. We found that the lowest-energy $LiFeSiO_4$ configurations corresponding to each Li_2FeSiO_4 structures all have 3 cations surrounding each oxygen atoms (1 Li + 1 Fe + 1 Si, see fig. 2 right) . The results agree with our assumption.

Using the structural rule discussed above for screening, the number of final candidate low-energy $LiFeSiO_4$ configurations for each Li_2FeSiO_4 considered is greatly reduced to less than 20 after removing duplicated configurations. Their energies are evaluated by DFT calculations after fully structure relaxations.

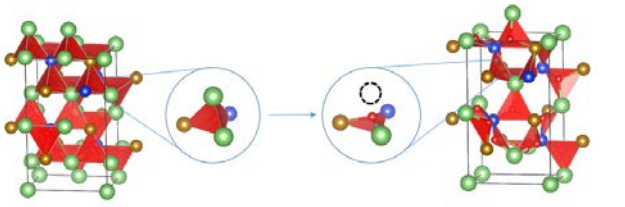

Fig. 2 Structural rules for Li_2FeSiO_4 and $LiFeSiO_4$. In the Li_2FeSiO_4 structures, each O atom has 2 Li + 1 Fe + 1 Si atoms surrounded. After removing half Li atoms, each O atom has 1 Li + 1 Fe + 1 Si atoms surrounded. The Oxygen-centered polyhedra are colored with red in order to show the coordination number.

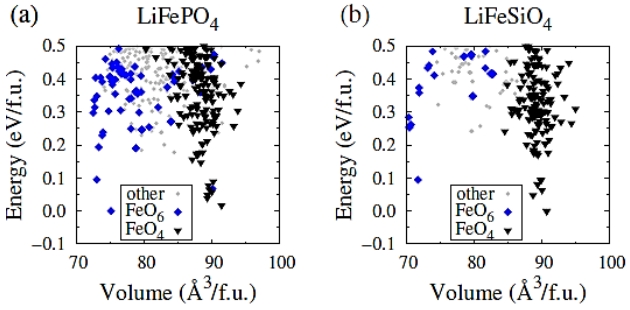

Fig. 3 The Energy vs Volume diagram of (a) $LiFePO_4$ structures (b) corresponding $LiFeSiO_4$ structures which are substituted from $LiFePO_4$ by changing P to Si. The blue squares represent FeO_6 type, black triangles represent FeO4 type, and gray dots represent other type. The y axis is the relative energy to the ground state of $LiFePO_4$ or $LiFeSiO_4$, respectively.

3.2 Source II. Generation of the substituted phases

The other source of $LiFeSiO_4$ structures is from the substitution of $LiFePO_4$, where we were able to identify a new group of structures which do not have well-defined vacancy sites to recover to a low-energy Li_2FeSiO_4 state. As discussed in our previous work[19], low-energy $LiFePO_4$ structures are constructed initially focusing on building Fe-P networks. Afterwards, O atoms are added around each P atom to form PO_4 tetrahedrons whose orientations are then optimized by force-field methods. Li atoms are finally added into the remaining vacancy sites of $FePO_4$ configurations. Details of this method can be find in the literature [19]. The previously searched $LiFePO_4$ structures are substituted with Si on P sites to generate low-energy $LiFeSiO_4$ structures.

Our $LiFePO_4$ structural database contains many low-energy $LiFePO_4$ phases with different types (fig. 3a). We substitute P atoms in $LiFePO_4$ structures with Si atoms and relax them with DFT. The energy and volume comparison between the $LiFePO_4$ structures and the corresponding $LiFeSiO_4$ structures are shown in fig.3. We can see that while $LiFePO_4$ prefer FeO_6 type structures (fig. 3a), $LiFeSiO_4$ (fig. 3b) prefer FeO_4 type. Most FeO_6 and other type structures move up in energy after replacing P with Si.

In order to show the rationality of the $LiFeSiO_4$ strcuture database construction from the substitution of $LiFePO_4$, i.e. the inheritance of energy order and structural properties, more specific diagrams comparing the energy or volume of individual low-energy structures before and after substitution are shown in figure 4. In fig. 4a and fig. 4b, we plot the energy of individual structures and a diagonal line with a gradient of 1.0 as reference. It can be seen that in FeO_6 type structures $LiFeSiO_4$ has systematically higher energy than the corresponding $LiFePO_4$ structure (fig 4b) while FeO_4 type structures show good correspondence between $LiFeSiO_4$ and $LiFePO_4$ (fig 4a). In fig. 4c, the volume is slightly bigger in $LiFeSiO_4$ compounds relative to $LiFePO_4$ while fig. 4d shows

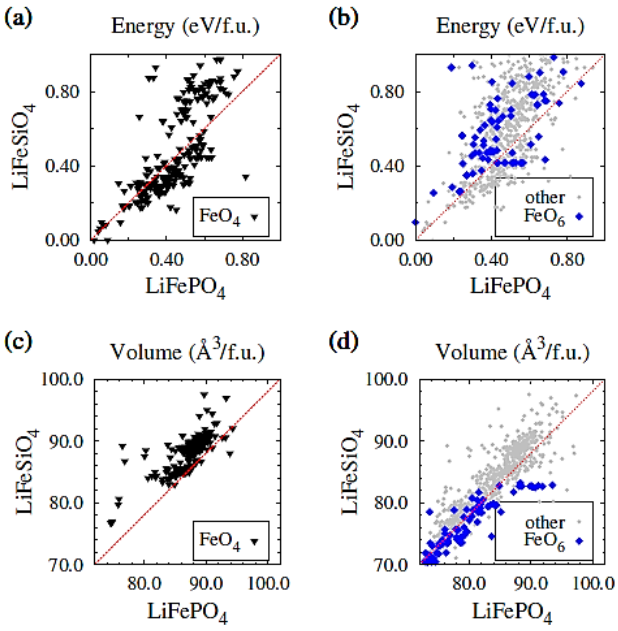

Fig. 4 Correlations between the energy and volume of $LiFePO_4$ and $LiFeSiO_4$. (a) the relative energy of FeO_4 type; (b) relative energy of FeO_6 and other type; (c) volume of FeO_4 type; (d) volume of FeO_6 and other type. The red diagonal lines' gradient is 1. In the energy, the value is relative to the ground state of each type ($LIFePO_4$ and $LiFeSiO_4$) in our structural pool

for FeO_6 types $LiFePO_4$ and $LiFeSiO_4$ volumes are more similar.

Among the many FeO_4 type $LiFeSiO_4$ phases, we discovered some low-energy structures that are good candidates as "trap" structures during the delithiation of Li_2FeSiO_4. When inserting more Li atoms to these special substituted $LiFeSiO_4$ structures, the corresponding fully lithiated Li_2FeSiO_4 have much higher energy than the original Li_2FeSiO_4. These special $LiFeSiO_4$ structures are what we call the "trap" phases since it is hard to insert Li back and return to the Li_2FeSiO_4 state in these structures.

To investigate the transition process into "trap" structures, we select similar $LiFeSiO_4$ structures between the Li-Fe site-exchange structural pool and the "trap" phases in the second dataset to calculate the transition barrier. The similar structures are topologically equal but with different levels of distortion in Fe-Si network and cell.

3.3 Phase transitions in $LiFeSiO_4$

We select 10 lowest-energy Li_2FeSiO_4 structures in the previous-developed database [18] (including 5 experimental phases, No.2:$P2_1/n$, No.3:$Pmn2_1$, No.6:$Pmn2_1$-cycled, No.8:$P2_1/n$-cycled, No.9: $Pmnb$) for removal of Li and site-exchange operations. The Li_2FeSiO_4 structures are numbered in order of energy as shown in fig 5a. Different symbols are used to denote structures with different types of Fe-Si networks (fig.1): structures 1,2,3 and 9 have 2D Fe-Si networks while 4,5 and 10 have 3D* networks and 6,7,8 have 3D type of networks.

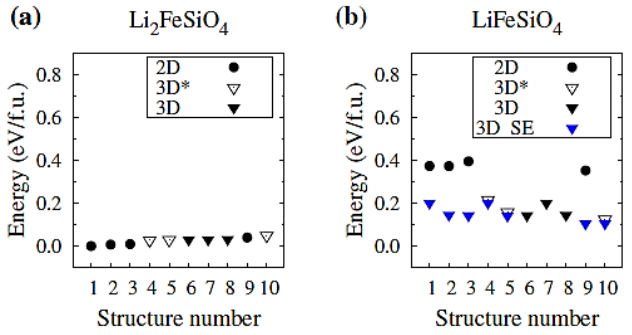

Fig. 5 (a) Energies of 10 lowest Li_2FeSiO_4 structures with different Fe-Si networks. (b) Energies of the corresponding $LiFeSiO_4$ structures which are from the delithiation and/or Li-Fe site-exchange in the 10 lowest Li_2FeSiO_4 structures in (a). Solid triangles represent 3D Fe-Si network, empty triangles for 3D* Fe-Si network, dots for 2D Fe-Si network. Blue color means the Li-Fe site-exchanged structure.

During the removal and addition of Li atoms to the cathode, if the Fe-Si network of the material remains intact during the charge/discharge cycle, the material can return continuously to its original condition and the process is reversible for many cycles. However, if the Fe-Si network suffers changes during the cycling process, it can leave the system trapped in structures which cannot return to the original fully Li-occupied state. Thus, in the following, we study changes in Fe-Si networks that can occur as Li atoms are removed and the system reaches the $LiFeSiO_4$ chemical composition. The lowest delithiated and Li-Fe site exchanged $LiFeSiO_4$ phase that corresponds to each Li_2FeSiO_4 are plotted in fig.5b. It can be seen that independent of the original Fe-Si network, the lowest energy structures after site-exchange all convert to 3D type Fe-Si networks indicated by solid-triangle symbols (see examples in fig.1b).

The 2D Fe-Si networks (fig. 1a) are energetically favourable in Li_2FeSiO_4 [18] but become quite unfavourable in $LiFeSiO_4$ (number 1,2,3 and 9 structures with solid dots in fig.5). From 2D to 3D, the energy drops about 0.2 eV/f.u. This 2D to 3D Fe-Si network transition is achieved by moving the Fe atoms to the Li vacancy sites, i.e. exchanging Fe atoms and Li vacancies.

The energies of 3D* type Fe-Si networks (fig. 1c) are slightly higher than 3D type. Exchange of Fe atoms and Li atoms will convert 3D* to 3D networks. Considering the margin of forward and inverse transition, the net transition rate of 3D* to 3D is probably much lower than the net transition rate of 2D to 3D due to the smaller energy difference of the former. In addition, since the final positions for the move are occupied, concerted motion of the atoms are required for this type of transition.

There are also structures (number 6, 7 and 8) that do not have a lower-energy Fe-Si network by Site-Exchange since the original Li_2FeSiO_4 are already in 3D type. Although the 3D type Fe-Si networks have the lowest energy among the 3 types of $LiFeSiO_4$, there still could be some potential structural transitions for these 3D Fe-Si networks beyond the mechanism of Li-Fe site-exchange, as shown in fig. 6.

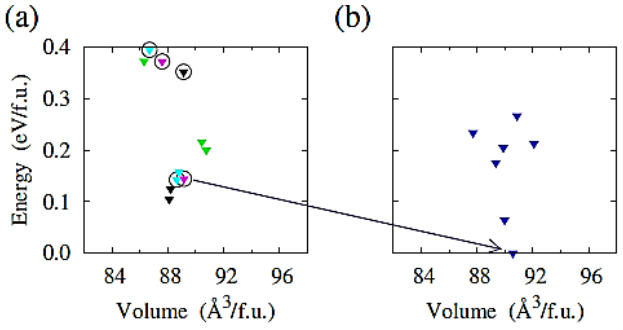

Fig. 6 Energy vs volume diagram of (a) $LiFeSiO_4$ structures from Li_2FeSiO_4 through delithiation or site-exchange and (b) "Trap" phases of $LiFeSiO_4$ substituted from $LiFeSiO_4$. Structures delithiated from the experimental Li_2FeSiO_4 phases are circled out in (a).

We combine all of the 17 $LiFeSiO_4$ structures listed in fig. 5 and examine their energy and volume behaviour in fig. 6a. After removing duplication, there are 11 distinct phases left. We sort them into 4 groups (fig. 6a represented with different colour) and each group has almost identical structures but with Fe and Li or Li vacancy sites exchanged between atom sites. After many successive Li-Fe site-exchange processes with charge-discharge cycling, the material will cycle between different structures in a group, and gravitate towards the lowest energy structure in each group. We note that all these structures correspond to delithiated phase from Li_2FeSiO_4 (some are Li-Fe site-exchanged, but they can be directly delithiated from other phases) and they can fully recover to the Li occupation of x=2. Such 'recovered' structures have energy within 0.06 eV/f.u. above the Li_2FeSiO_4 ground state. Therefore, transformation to these structures with cycling will not cause degradation in the charge capacity of the material.

The energy vs volume relation of the "trap" structures obtained from Si substitution of the $LiFePO_4$ structure database is plotted in fig. 6b. When these "trap" phases are inserted with Li atoms and discharged back to Li_2FeSiO_4, configurations with energies 0.4 eV/f.u higher than the Li_2FeSiO_4 ground state are resulted. The vacancy sites in those "trap" structures forbid the inserted Li atoms forming LiO_4 tetrahedra or make them too close to other

Considering the lowest energy "trap" structure in fig. 6b which has an energy ~0.1eV/f.u. lower than the population produced by reversible cycling (in fig. 6a). To get a picture of the transition from reversible structures to the lowest energy "trap" structure, we located a structure in fig. 6a: the half-delithiated experimental P21/n-cycled phase that is topologically equivalent to the "trap" phase but differs in the distortions of the Fe-Si network and also has slightly different unit cells (see arrow in fig 6) i.e. transition between the two structures can occur via small atomic motions with an accompanying strain of the material. The structural information of this selected "trap" phase is shown in Tab.1.

When we reinsert Li atoms back into these two phases we find that they have quite different energies as well as different atomic pair distributions around the Li atoms. Pair distribution functions between Li and other atoms are plotted in fig. 7 for

Space Group Number 7

cell		a	b	c
		8.58859	5.19086	8.50025
		alpha	beta	gamma
		90.0000	107.2419	90.0000
Atom	wyckoff	x	y	z
Li	2a	0.00042	0.83640	0.00017
Li	2a	0.51352	0.67613	0.65632
Fe	2a	0.75623	0.82836	0.23891
Fe	2a	0.26432	0.67263	0.89295
Si	2a	0.38604	0.81867	0.26548
Si	2a	0.88198	0.67785	0.62450
O	2a	0.35678	0.66252	0.42269
O	2a	0.72901	0.81929	0.67263
O	2a	0.54838	0.30141	0.72530
O	2a	0.04446	0.26237	0.27930
O	2a	-0.09935	0.81428	0.45657
O	2a	0.23330	0.76309	0.09897
O	2a	0.40586	0.87105	0.80401
O	2a	0.85113	0.63418	0.10018

Tab. 1 The structure information of the selected "trap" phase. The unit cell is monoclinic and atom positions are represented in direct coordination.

both phases. It can be seen that environment for the additional Li atoms in the "trap" phase (fig. 7b) has a number of violations compared with low-energy Li_2FeSiO_4 structures (fig. 7a). The inserted Li atoms (grey atoms in fig.7b) are too close to other Li atoms (see red line in fig, 7b denoting the Li-Li pair distribution function). Also, when connected with the

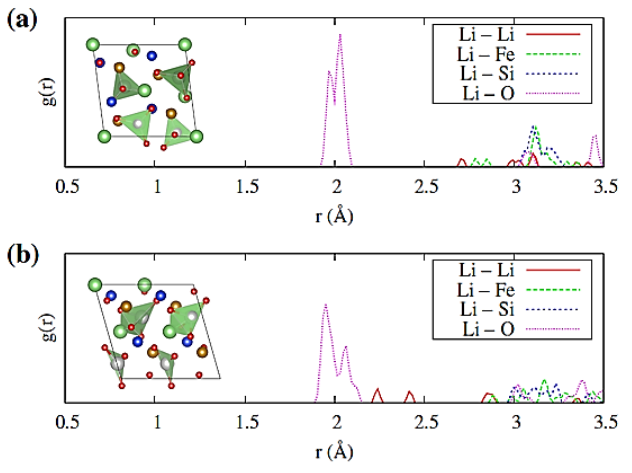

Fig. 7 Pair distribution of the two similar structures in fig.6a and 6b (the vacancy sites are inserted with more Li atoms to Li_2FeSiO_4 state). (a) the experimental P21/n-cycled Li_2FeSiO_4 phase. (b) the lithiated compound based on the "trap" phase. More Li atoms are inserted in the $LiFeSiO_4$ structures. We marked the newly inserted Li atoms with "grey" color and plot the Li-O polyhedron in order to show the environment.

neighbour atoms, some inserted Li atoms connect to the other Li atoms (see structures in fig. 7b) and some cannot form a LiO_4 tetrahedron.

In fig. 8 we can see that both of the $P2_1/n$-cycled phase and the "trap" phase have same 3D type Fe-Si network but with different levels of distortion. On the top point in pathway (see the top structure among the 3 in fig.8), some Fe-Si bonds are not as parallel as in the beginning, but they are closer to the left $P2_1/n$-cycled phase than to the right "trap" phase, indicating the transition direction is easier from left to right than inverse. The calculated transition barrier from the $P2_1/n$-cycled phase to the "trap" phase is about 0.50 eV (28 atoms) which is relatively low compared to the inverse direction (0.86 eV), also indicating a possible phase transition. Note that the transition barrier calculation is done at x=1 of Li_xFeSiO_4 for convenience, but the actual composition where phase transition happens is not clear and there exists the possibility to find an x value of Li_xFeSiO_4 where the corresponding barrier is smaller than 0.5 eV.

The $LiFeSiO_4$ structures delithiated from the five experimentally observed Li_2FeSiO_4 phases are drawn with their inner Fe-Si networks in fig.9 to show their structural relationships. Form 2D to 3D, Fe atoms motion to Li vacancy sites drop the energy by about 0.2 eV/f.u. From 3D to "trap" phase, the energy is further lowered, however, distortions in the Fe-Si network and lattice strain associated with the structural transition affect the environments of the Li vacancy sites, making it harder to reinsert the removed Li atoms. The XRD spectrum of the "trap" phase is simulated and plotted in Fig. 10 for future experimental comparisons.

We also proposed a new phase (fig. 9f) that can occur during cycling of the half delithiated Pmnb experimental structure (fig. 9c). The structural information of this new phase is shown in supplementary material.

Conclusion

We examined structural phase transitions that can occur in the Li_xFeSiO_4 (x=0~2) system when x decreases to 1. The Li-Fe site-exchange process among different Fe-Si networks is investigated for $LiFeSiO_4$. From 2D to 3D Fe-Si networks, the actual transition mechanism is the exchange of Li vacancy sites and Fe atom sites (i.e. Fe atoms move to nearby Li vacancy sites). While from 3D* to 3D Fe-Si networks, the exchange happens between Li and Fe atoms sites. The transition from 2D to 3D Fe-Si networks is accompanied by a big energy drop while from 3D* to 3D has little energy change. Using the site-exchange rules we discovered, we proposed a new cycled structure for the experimental Pmnb phase in fig. 9f and fig. 10b (different from the $Pmn2_1$-cycled phase).

After the initial phase transition from 2D to 3D Fe-Si network, additional phase transitions can land the system in "trap" structures with $LiFeSiO_4$ composition that cannot be converted back to the original Li_2FeSiO_4 state, causing degradation of the cathode capacity. Candidates for these "trap" structures are investigated in searches where substitution of Si for P in a previously developed structural database for the $LiFePO_4$ system. In these new phases, insertion of Li atoms

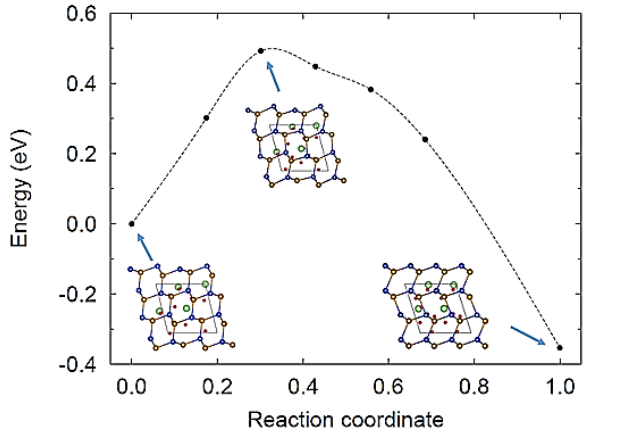

Fig. 8 NEB transition barrier between the $P2_1/n$-cycled phase (left) and "trap" phase (right). Changes of the Fe-Si networks in the transition pathway are also plotted.

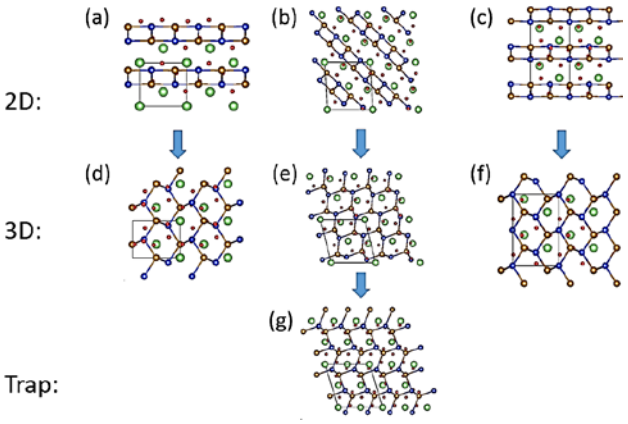

Fig. 9 Phase transition between half-delithiated structures from 5 experimental phases and the "trap" phase. (a) $Pmn2_1$ (b) $P2_1/n$ (c) $Pmnb$ (d) $Pmn2_1$-cycled (e) $P2_1/n$-cycled (f) possible cycled phase of $Pmnb$ (g)"trap" phase.

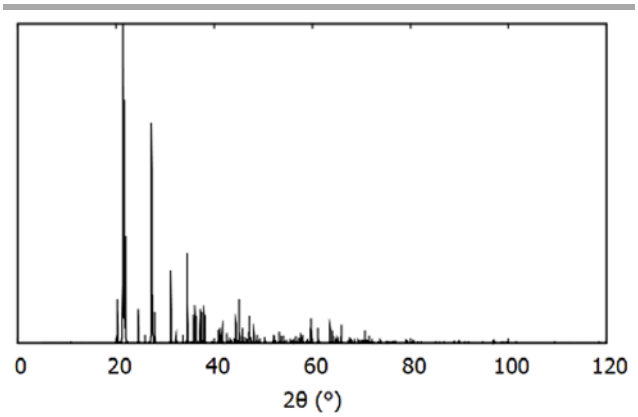

Fig. 10 Simulated XRD spectrum of the "trap" phase using Cu K\alpha radiation and the structure information listed in Tab. 1. the full width at half maximum is of the peaks is set to 0.05 degree.

produces new Li_2FeSiO_4 structures with much higher energy than the Li_2FeSiO_4 ground state. These substituted phases form "trap" phases that cannot go back to Li_2FeSiO_4 during the discharging process. We found eight "trap" phases and one of them is topologically equal to the experimental P21/n-cycled phase (fig. 6b) but with different levels of distortion in Fe-Si network and unit cell. They have the same type of 3D diamond-like Fe-Si networks. The transition barrier is relatively low compared to that of inverse direction, which indicates this capacity-damaging phase transition could happen in experiment.

Acknowledgements

Z. Lin acknowledges the supports of the National Natural Science Foundation of China (11574284 & 11774324), National Basic Research Program of China (973 Program 2012CB215405) and Collaborative Innovation Center of Suzhou Nano Science and Technology. X. Lv acknowledges the support from USTC and China Scholarship Council (File No. 201506340115). Work at Ames Laboratory was supported by the US Department of Energy, Basic Energy Sciences, Division of Materials Science and Engineering, under Contract No. DE-AC02-07CH11358, including a grant of computer time at the National Energy Research Supercomputing Center (NERSC) in Berkeley, CA. Work at Xiamen University was supported by the National Key Research Program of China (Grant No. 2016YFA0202601). K.M. Ho acknowledges the support from the 111 Project (No. B13027) and USTC Qian-Ren B (1000-Talents Program B) fund.

Reference

1 A. Nytén, A. Abouimrane, M. Armand, T. Rn Gustafsson and J. O. Thomas, *Electrochem. commun.*, 2005, **7**, 156–160.
2 H.-N. Girish and G.-Q. Shao, *RSC Adv.*, 2015, **5**, 98666–98686.
3 A. R. Armstrong, N. Kuganathan, M. S. Islam and P. G. Bruce, *J. Am. Chem. Soc.*, 2011, **133**, 13031–13035.
4 C. Sirisopanaporn, C. Masquelier, P. G. Bruce, A. R. Armstrong and R. Dominko, *J. Am. Chem. Soc*, 2011, **133**, 1263–1265.
5 T. Muraliganth, K. R. Stroukoff and A. Manthiram, *Chem. Mater*, 2010, **22**, 5754–5761.
6 D. Lv, W. Wen, X. Huang, J. Bai, J. Mi, S. Wu and Y. Yang, *J. Mater. Chem.*, 2011, **21**, 9506.
7 Z. Gong and Y. Yang, *Energy Environ. Sci.*, 2011, **4**, 3223.
8 J. Yang, J. Zheng, X. Kang, G. Teng, L. Hu, R. Tan, K. Wang, X. Song, M. Xu, S. Mu and F. Pan, *Nano Energy*, 2016, **20**, 117–125.
9 A. Nytén, S. Kamali, L. Häggström, T. Gustafsson and J. O. Thomas, *J. Mater. Chem.*, 2006, **16**, 2266–2272.
10 L. Li, L. Zhu, L.-H. Xu, T.-M. Cheng, W. Wang, X. Li and Q.-T. Sui, *J. Mater. Chem. A*, 2014, **2**, 4251–4255.
11 P.Zhang, Y.Zheng, S.Yu, S.Q.Wu, Y.H.Wen, Z.Z.Zhu and Y.Yang, *Electrochim. Acta*, 2013, **111**, 172–178.
12 P. Zhang, C. H. Hu, S. Q. Wu, Z. Z. Zhu, Y. Yang, P.Zhang, C.H.Hu, S.Q.Wu, Z.Z.Zhu and Y.Yang, *Phys. Chem. Chem. Phys.*, 2012, **14**, 7346–7351.
13 T. Kojima, A. Kojima, T. Miyuki, Y. Okuyama and T. Sakai, *J. Electrochem. Soc.*, 2011, **158**, A1340.
14 D.-H. Seo, H. Kim, I. Park, J. Hong and K. Kang, *Phys. Rev. B*, 2011, **84**, 220106.
15 A. Saracibar, A. Van der Ven and M. E. Arroyo-de Dompablo, *Chem. Mater.*, 2012, **24**, 495–503.
16 C. Eames, a R. Armstrong, P. G. Bruce and M. S. Islam, *Chem. Mater.*, 2012, **24**, 2155–2161.
17 D. Lv, J. Bai, P. Zhang, S. Wu, Y. Li, W. Wen, Z. Jiang, J. Mi, Z. Zhu and Y. Yang, *Chem. Mater.*, 2013, **25**, 2014–2020.
18 X. Zhao, S. Wu, X. Lv, M. C. Nguyen, C.-Z. Wang, Z. Lin, Z.-Z. Zhu and K.-M. Ho, *Sci. Rep.*, 2015, **5**, 15555.
19 X. Lv, X. Zhao, S. Wu, P. Wu, Y. Sun, M. C. Nguyen, Y. Shi, Z. Lin, C.-Z. Wang and K.-M. Ho, *J. Mater. Chem. A*, 2017, **5**, 14611–14618.
20 Z. Ye, X. Zhao, S. D. Li, S. Q. Wu, P. Wu, M. C. Nguyen, J. H. Guo, J. X. Mi, Z. L. Gong, Z.-Z. Z. Zhu, Y. Yang, C.-Z. Z. Wang and K.-M. M. Ho, *Electrochim. Acta*, 2016, **212**, 934–940.
21 P. Wu, S. Q. Wu, X. Lv, X. Zhao, Z. Ye, Z. Lin, C. Z. Wang and K. M. Ho, *Phys. Chem. Chem. Phys.*, 2016, **18**, 23916–23922.
22 G. Kresse and J. Furthmüller, *Phys. Rev. B*, 1996, **54**, 11169–11186.
23 J. P. Perdew, K. Burke and M. Ernzerhof, *Phys. Rev. Lett.*, 1996, **78**, 1396–1396.
24 S. L. Dudarev, S. Y. Savrasov, C. J. Humphreys and a. P. Sutton, *Phys. Rev. B*, 1998, **57**, 1505–1509.
25 H. J. Monkhorst and J. D. Pack, *Phys. Rev. B*, 1976, **13**, 5188–5192.
26 G. Henkelman, B. P. Uberuaga and H. Jónsson, *J. Chem. Phys.*, 2000, **113**, 9901.
27 K. Momma and F. Izumi, *J. Appl. Crystallogr.*, 2011, **44**, 1272–1276.